60S subunit joining exposes nascent pre-40S rRNA for quality control.

Jay Rai[1,2], Melissa D. Parker[2,3], Haina Huang[3], Stefan Choy[3], Homa Ghalei[3,4], Matthew C. Johnson[1,5], Katrin Karbstein[3,6*] and M. Elizabeth Stroupe[1*]

[1] Department of Biological Science and the Institute of Molecular Biophysics, Florida State University, Tallahassee, Florida, 32306
[2] These authors contributed equally
[3] Department of Integrative Structural and Computational Biology, The Scripps Research Institute, Jupiter, Florida, 33458
[4] Present address: Emory University School of Medicine, Department of Biochemistry, Atlanta, Georgia
[5] Present address: University of Washington, Department of Biochemistry, 1959 NE Pacific Street, Box 357350, Seattle, WA 98195
[6] HHMI Faculty Scholar
* To whom correspondence should be addressed: Katrin Karbstein and M. Elizabeth Stroupe

Email: kkarbst@scripps.edu; mestroupe@bio.fsu.edu

ORCIDs: Stroupe: 0000-0002-4393-1951

Classification

Biological Sciences, Biophysics and Computational Biology

Keywords

Ribosome assembly, small ribosome subunit, cryo-EM

Author Contributions

J.R. and H.G. prepared samples; J.R. and M.E.S. carried out structure reconstruction; M.D.P., H.H. and S.C. carried out yeast analyses; M.C.J. performed cryo-EM analysis of pre-40S; K.K. and M.E.S. conceived of the experiments and wrote the paper.

This PDF file includes:

Main Text
Figs. 1 to 4

Abstract

During their maturation, nascent 40S subunits enter a translation-like quality control cycle, where they are joined by mature 60S subunits to form 80S-like ribosomes. While these assembly intermediates are essential for maturation and quality control, how they form, and how their structure promotes quality control remains unknown. To address these questions, we determined the structure of an 80S-like ribosome assembly intermediate to an overall resolution of 3.4 Å. The

structure, validated by biochemical data, resolves a large body of previously paradoxical data and illustrates how assembly and translation factors cooperate to promote the formation of an interface that lacks many mature subunit contacts but is stabilized by the universally conserved Dim1. The structure also shows how this interface leads to unfolding of the platform, which allows for temporal regulation of the ATPase Fap7, thus linking 40S maturation to quality-control during ribosome assembly.

Significance Statement

Until now, knowledge of the structure-function relationships guiding the translation-like quality control cycle that directs 80S ribosome maturation has been minimal. Here, we report the 3.4 Å-resolution structure of an 80S-like intermediate, showing a substantially remodeled interface and platform that positions the subunits in a more extreme classic state, testing the ability of nascent ribosomes to undergo the motions of translocation.

Main Text

Introduction

Ribosome assembly is a highly regulated process, beginning with transcription, processing, and folding of the rRNA in the nucleolus. Binding of most ribosomal proteins is coupled to these co-transcriptional events, facilitated, coordinated, and regulated via a machinery of nearly 200 assembly factors (AFs) that bind transiently to nascent ribosomes. After completing the co-transcriptional events, largely assembled precursors retaining seven AFs are exported into the cytoplasm to undergo final maturation (1, 2). These final steps are coupled to quality control in a translation-like cycle where pre-40S ribosomes bind mature 60S subunits in an eIF5B-dependent manner to produce 80S-like ribosomes (3-5), the substrates for quality control by the essential ATPase Fap7. By binding 80S-like ribosomes and inducing structural changes that release the AF Dim1, Fap7 tests the ability of newly-made ribosomes to adopt conformations critical to translocation of the mRNA. Bypass of this step allows release of defective ribosomes into the translating pool (5).

Recently, structural information on very early nucleolar (6-8), as well as initial cytoplasmic 40S assembly intermediates (9-13), has become available. However, the structure of 80S-like ribosomes has not been described despite their central role for quality control and maturation. Thus, how they are formed despite the presence of AFs that block subunit joining remains unclear. Furthermore, how they enable temporal regulation of Fap7 activity is also unknown.

We used single-particle cryogenic electron microscopy (cryo-EM) to visualize the structure of 80S-like ribosomes that accumulate upon Fap7 depletion (5). The structure is validated by biochemical data herein, as well as previous structural and biochemical data, and illuminates how 80S-like ribosomes harboring Dim1 and Tsr1 form, despite their position blocking subunit joining in earlier intermediates. Furthermore, structural and biochemical data also reveal how 80S-like ribosomes enable quality control.

Results and Discussion

Highly mobile 80S-like ribosomes

To better understand how 40S ribosome maturation is quality-controlled via structural and functional mimicry of translation events, we used cryo-EM to visualize the structure of 80S-like ribosomes. These ribosome assembly intermediates were accumulated by Fap7 depletion (4, 5) and purified via a TAP-tag on Tsr1 (5). SDS-PAGE analysis, mass-spectrometry, and Western blot analysis demonstrate that these intermediates retain the AFs Tsr1, Dim1, and Pno1, but Nob1 is substoichiometric (**Fig. S1a)**. Additionally, 60S ribosomal proteins and ribosome associated factors like the SSA/SSB chaperones were identified, consistent with the presence of 25S rRNA (5). Importantly, previous biochemical data confirmed that these intermediates are on pathway because addition of recombinant Fap7/ATP releases Dim1 and forms a hybrid-like state (14).

Initial classification identified two populations of particles. One refined to a resolution of 3.6 Å and had features like mature 80S ribosomes (**Fig. S1b-d**), similar to a recently noted 80S pre-ribosome lacking AFs (12). This subclass lacks Tsr1, Dim1, and Pno1; its platform, beak, decoding helix, and B3 bridge are in their mature conformation; and there is no density for any tRNA (**Fig. S1e**). This subclass is not described further as its significance is unclear.

The other subclass had strong 60S, but weaker pre-40S, density (**Fig. S1b-d**). Further refinement of either subunit improved the clarity of pre-40S to an overall resolution of 3.7 Å and 60S to an overall resolution of 3.4 Å (**Fig. S1f**). Although the particles showed no preferred orientation, the resolution of pre-40S remained anisotropic (**Fig. S1g-j)**. Local classification described below clarified the interface and platform to ~5.5-8.5 Å-resolution (**Fig. S1k-l**).

Pre-40S movements

Improvement of pre-40S upon refinement indicated that it is mobile. Multi-body analysis (15) showed three main motions (**Fig. S2a**), where pre-40S rotates out from 60S and parallel to the interface (**Fig. S2b**), freed by fewer subunit bridges (**Fig. S3**). Pre-40S moves as a rigid body, in contrast to mature 40S where the head moves independently (15), perhaps because Tsr1 binds and holds together the body and head. Additionally, or alternatively, the neck, which is the point of head movement, has not yet formed. The first Eigen vector describes motions that resemble extreme translocation movements. Further, the position of pre-40S relative to 60S is consistent with footprinting, which showed that 80S-like ribosomes are in a classic-like state (14). In fact, 80S-like ribosomes appear hyper-classic in the composite assembly, 23° from the rotated state (**Fig. S4**).

Immature subunit interface

Previous structural analyses demonstrated that Dim1 and Tsr1 inhibit subunit joining. Dim1 sterically blocks 60S binding (10-13). Tsr1 blocks eIF5B and stabilizes a conformation of h44 that is "pulled out" from the subunit interface, thereby clashing with 60S and perturbing subunit bridges on h44 (10-13). To accommodate these AFs and h44, pre-40S is opened away from 60S, creating space between the subunits to allow movement of Tsr1 and Dim1 relative to their position in isolated pre-40S (**Fig. 1a-c**). Consequently, the 80S-like subunit interface is formed by fewer bridges than in mature 80S. For example, the B1a/b/c bridges, which involve the 40S head, are not yet formed because the pre-40S head is far from the 60S central protuberance (**Fig. 1c and S3**). Similarly, pre-40S turns away from 60S on the platform side, and towards it on the beak side, thus bridge B7a cannot form because that side of the head is too distant from 60S. Further, the twisted position of pre-40S relative to 60S accommodates the immature position of h44, which is shifted left, preventing formation of the B3 and B5 bridges at the top of h44 (10, 12). In contrast, eukaryote-specific bridges at the 40S foot are largely maintained. In the case of a B5/B8-like bridge between h44 and Rpl23/uL14 and a B6-like bridge between h44 and Rpl24, the inter-subunit connections shift due to the novel orientations of the subunits but involve analogous interactions between similar structural elements (**Fig. S5**).

A striking difference between 80S-like and mature 80S ribosomes is the change in interaction between H69 and pre-40S. H69 is the target of RRF (16), which dissociates ribosomes, as well as some antibiotics (17-19), and forms an A-minor interaction with h44 (20) to establish the B2a bridge, stabilizing 80S ribosomes. In contrast, in 80S-like ribosomes, H69 binds h24 (**Fig. 1d-e**), which moves substantially from its mature position, as follows. Although the moderate resolution

of the subunit interface prevents us from precisely modeling atomic interactions between H69 and h24, two helical densities can be assigned to H69 and h24 with high confidence. The local resolution of one helix is ~5.5 Å, lower than 60S but sufficiently well-resolved to model H69 in its mature position (**Fig. 1e and S1k**). The tip of the other helix is resolved at ~8.5 Å; however, it connects to the well-resolved base of a repositioned h24, strongly suggesting that the RNA that binds H69 derives from h24 (**Fig. 1e and S1k**). Notably, we validated interactions between Dim1 and h24, as well as Dim1 and 60S, in biochemical experiments described below.

Dim1 stabilizes h24 and binds 60S

In pre-40S, Dim1 sterically blocks approach of H69 from 60S, inhibiting subunit joining (10-13). If Dim1 stayed at that position in 80S-like ribosomes, it would still block subunit joining despite the remodeled interface because H69 remains the main subunit connection. Although the resolution of Dim1 is at ~8.5 Å despite local classification, the map shows that Dim1 repositions with h24, moving above H69 to alleviate the steric conflict (**Fig. 2a and Movie S1**). This movement essentially releases Dim1 from pre-40S, maintaining contact with h24 while promoting its interaction with 60S, thus priming Dim1 for release.

To validate the position of Dim1 and probe the importance of contacts between Dim1 and h24, as well as Dim1 and 60S, we created Dim1 variants and tested their effects on subunit joining. Residues altered in Dim1-FRK (F231L/R233E/K234E) face h24 in 80S-like, but not pre-40S, ribosomes (**Fig. 2b-c**). Residues altered in Dim1-IKN (I250A/K253A/N254A) face across the interface toward Rpl11 and the C-terminus of Rpl42 (**Fig. 2b-c**). These residues do not form major interactions in pre-40S ribosomes. To test if the altered residues are important for subunit joining, we used an *in vivo* assay for 80S-like ribosome formation. The variants were expressed in a galactose-inducible/glucose-repressible Dim1/Fap7 yeast strain, supplemented with plasmids encoding wild-type or variant Dim1 and no or inactive Fap7. In strains competent for 80S-like ribosome formation, accumulates of 80S-like ribosomes upon depletion or inactivation of Fap7 leads to co-sedimentation of pre-18S and 25S rRNA in 80S-sized fractions (4, 5). Both Dim1-FRK and Dim1-IKN impair formation of 80S-like ribosomes (**Fig. 2d-e)**. Thus, these biochemical data validate interactions between Dim1 and both h24 and 60S, establishing a role for Dim1 in stabilizing 80S-like ribosomes.

Tsr1 promotes the opened interface

In earlier 40S assembly intermediates, Tsr1 binds between the body and head, with its N-terminal α-helix inserted behind h44 to force it away from the body, blocking formation of canonical 80S ribosomes (10-13, **Fig. S6a**). In 80S-like ribosomes, the C-terminal domain is no longer attached to the head, but repositioned towards the beak's tip via a rigid-body movement around a hinge at Ala63 within the N-terminal helix, which remains under h44 (**Figs. 3a, S6b-c, and Movie S2**).

To test the importance of this hinge rotation, we deleted the Tsr1 N-terminal helix (Tsr1-ΔN74) and assessed the effect on cell growth and formation of 80S-like ribosomes. In yeast strains where endogenous Tsr1 is under a galactose-inducible/glucose-repressible promoter, providing Tsr1-ΔN74 on a plasmid produces a lethal growth phenotype (**Fig. S6d).** We further used the *in vivo* assay described above to assess 80S-like ribosome formation in the hinge-helix deletion strain. Formation of 80S-like ribosomes is blocked in the eIF5B deletion strain (4); similarly, formation of 80S-like ribosomes is blocked by truncating Tsr1, as shown by loss of pre-40 and 60S subunits co-sedimentation upon Fap7 depletion in the Tsr1-ΔN74 strain (**Fig. 3b**)**.** Thus, rotation around the hinge in Tsr1 is essential for the formation of 80S-like ribosomes.

In our previous dataset of earlier 40S assembly intermediates (11), Tsr1 appears similarly rotated in a small population of molecules (**Fig. S7a**). In this low-resolution structure, Tsr1 has a disordered C-terminal domain due to its mobility in isolated pre-40S and/or the low number of particles. Nonetheless, this observation suggests that Tsr1's movement away from h44 and the beak is intrinsic to Tsr1, although not induced, but perhaps stabilized, by eIF5B.

The position of Tsr1 in previously described earlier pre-40S intermediates is incompatible with eIF5B binding (21). Nonetheless, eIF5B is required for formation of 80S-like ribosomes but has dissociated in a GTPase-dependent manner before this intermediate accumulates (3, 4). To visualize if Tsr1 repositioning enables eIF5B binding, we superimposed 60S from the mature 80S•eIF5B complex onto this intermediate to place eIF5B (22, **Figs. 3c-d and S6e-f**). This analysis suggests that the postulated clashes between Tsr1 and eIF5B (21) are largely resolved in these 80S-like ribosomes. Surprisingly, Tsr1 repositioning alone does not provide the steric relief but, rather, the opened subunit interface provides space for concurrent binding of eIF5B behind Tsr1 at the subunit interface.

The structure of 80S-like ribosomes clarifies multiple roles for Tsr1 in the formation of 80S-like ribosomes versus canonical 80S ribosomes: first, Tsr1 forces out h44, thereby sterically preventing the subunits from close approach to form the canonical subunit bridges in the head (**Figs. 1a and**

S6b); second, Tsr1 stabilizes the interface due to its interaction with both pre-40S and 60S (**Fig. S7b)**; third, Tsr1 blocks access of eIF5B to its typical binding site on 40S, instead enforcing a position that blocks formation of the B3 bridge (**Fig. 3c-d**). The B3 bridge is a strong and early-forming bridge (23), therefore Tsr1 steers the subunits into 80S-like ribosomes by promoting that different eIF5B position. While Dim1 stabilizes 80S-like ribosomes, Tsr1 induces formation of these complexes.

Head folding in nascent pre-40S

Previous structures showed that earlier pre-40S lack Rps10/eS10, Rps26/eS26, and Asc1 (10-13), and that the tip of h31 remains unfolded (10, 12). In 80S-like intermediates, Asc1 and Rps10 locate to their mature position (**Fig. S8**), indicating these proteins are recruited prior to Fap7 activity, as expected from previous biochemical analyses (4). Furthermore, the tip of h31 is visible (**Fig. S9**). This coincides with the beak moving to its mature position while the overall head straightens (**Fig. S10**), movements that originate where the head joins the body near the Tsr1 and Rio2 binding sites: in earlier pre-40S intermediates, Tsr1 binds immediately adjacent to the last ordered nucleotide in h31, and Rio2 binds adjacent to the h31's mature location (10-13). We suggest that these changes arise from dissociation of Rio2 and detachment of Tsr1 from the head, indicating roles for these maturation events in promoting h31 folding.

Platform unfolding

Extensive differences between earlier pre-40S subunits and 80S-like ribosomes are also observed at the platform, where a rigid body motion opens the platform towards 60S (**Fig. 4a**). This movement is presumably facilitated by repositioning of h24 from the platform to the subunit interface, accompanied by disorder in the tip of h23 and partial loss of Rps1 and Rps14, as previously observed (4), requiring local classification to improve its resolution. The other 80S ribosome subclass we observe has a canonical platform (**Fig. S1e**), ruling out artifacts during sample preparation as causative for the rearrangements. Further, the particles do not adopt a preferred orientation in the ice (**Fig. S1g**), as expected if they were interacting with the air-water interface thus unfolding the platform. We therefore conclude that these changes represent folding transitions during 40S subunit maturation.

To interpret the platform density, we placed Rps1•Rps14•Pno1 from the earlier pre-40S intermediates in the platform density with rigid body fitting, assuming the Rps14•Pno1 dimer

remained unaltered (**Fig. 4a**). To validate this assumption, we produced mutants in the Rps14•Pno1 interface, Rps14-R107E and Pno1-QDF (Q153E/D157R/F237A, **Fig. 4b**). These variants were tested for their effects on cellular growth in galactose-inducible/glucose-repressible Rps14 and Pno1 strains, respectively. Both variants demonstrated growth phenotypes (**Fig. S11a-b**). Because both are bound (but do not yet interact) in early 90S precursors (6-8), we used Northern analysis to confirm that these mutations do not affect early maturation events. Rps14 or Pno1 depletion leads to assembly defects that preclude formation of 20S rRNA (23-25, **Fig. S11c-d**). Rps14-R107E and Pno1-QDF produce 20S rRNA to nearly wild-type levels. Thus, lethal or near-lethal growth defects from these mutants do not arise from early maturation defects. Next, we used sucrose-gradient fractionation to ask if Pno1 is bound more weakly to 80S-like ribosomes in these mutants. 80S-like ribosomes were accumulated via depletion of Fap7 as described above (4), and Western analysis was used to probe the sedimentation of Pno1 with 40S or 80S ribosomes, or dissociated Pno1. As expected from a weakened Pno1•Rps14 interface, the fraction of free Pno1 increases in both mutants (**Fig. 4c-d**). These data strongly suggest that the Pno1•Rps14 interface is maintained in 80S-like ribosomes, supporting placement of the unchanged Rps1•Rps14•Pno1 complex in the platform density**.**

Further analysis of this opened platform illuminates the function of the ATPase Fap7 in the release of Dim1 (5). Fap7 bridges Dim1 and Rps14, presumably reflecting recruitment of Fap7 by Rps14 to promote Dim1 release (5). Thus, we asked if Fap7 could fit between Dim1 and Rps14. By superimposing the crystal structure of Fap7•Rps14 (24) onto Rps14, Fap7 is positioned adjacent to Dim1 (**Fig. 4e**), as predicted biochemically (5). Intriguingly, only one of the two observed Fap7•Rps14 interfaces places Fap7 in 80S-like ribosomes – the other clashes with the platform (**Fig. S12a-b**).

To validate the position of Fap7, we created mutations in Fap7 and Rps14 that would affect this interface. Rps14-K49E and Fap7-RYD (R114E/Y116A/D118K) alter residues that contact their binding partners only in the dockable interface, whereas Rps14-RVM (R41E/V42L/M46A) alters an arginine that binds Fap7 in both (Val42 and Met46 bind Fap7 in the dockable interface) (**Figs. 4e, S12c**). Each mutation results in a substantial growth phenotype (**Fig. S12d**). Furthermore, recombinant Fap7-RYD and Rps14-RVM fail to bind Rps14 and Fap7, respectively (**Fig. 4f**). Finally, as in inactive Fap7(5), the growth phenotype from Fap7-RYD is partially rescued by a self-releasing Dim1 mutation, Dim1-EKR (**Fig. 4g**). Together, these experiments support this placement of Fap7 in 80S-like ribosomes. Additionally, this biochemically-validated position of

Fap7 between Rps14 and Dim1 also validates interpretation of the medium-resolution features of the map: Rps14 on the platform and Dim1 at the subunit interface.

Fap7 binds Rps14 (5, 24, 25), and the biochemical data above demonstrate the importance of their interaction for Fap7's function in 40S maturation and Dim1 release (5). Rps14 is found at its mature position in the earliest 40S assembly intermediates (6-8), thus raising the question how temporal regulation of Fap7 recruitment to nascent ribosomes is achieved. Docking Fap7 onto earlier pre-40S intermediates demonstrates that it would clash with the tip of h23 within the platform (**Fig. S12b**). In contrast, in 80S-like ribosomes this steric conflict is relieved by opening of the platform, which repositions Rps14, and mobilizes h23. Thus, unfolding of the platform in 80S-like ribosomes allows for temporal regulation of Fap7 binding and activity to 80S-like ribosomes (**Fig. 4h**).

In summary, the structure of 80S-like ribosomes presented here, validated by genetic and biochemical data herein, as well as previous biochemical (5), mass spectrometry (4), and crystallographic (24) data, reveal unexpected features that allow for reconciliation and explanation of many previous observations. (i) 80S-like ribosomes display an opened interface whose formation is enabled by Tsr1. Tsr1 blocks the canonical binding mode of eIF5B, required for subunit joining; supports a conformation of the decoding helix that necessitates an open interface; and stabilizes the complex by binding both subunits. (ii) The most unexpected feature of the subunit interface in 80S-like ribosomes is the novel interaction of H69 from 60S with h24 from pre-40S, stabilized by Dim1. Because h24 is a component of the platform, this interaction opens the platform towards 60S and mobilizes constituent RNAs and proteins. (iii) Platform remodeling allows for temporal regulation of the ATPase Fap7, which functions in quality control of nascent 40S by linking dissociation of Dim1 to the ability to undergo conformational changes associated with translation (5). Thus, this structure finally explains how formation of 80S-like ribosomes is required for proofreading of 40S ribosome maturation.

Materials and Methods

Yeast strains/cloning: Yeast strains (**Table S1**) were produced using PCR-based recombination (26), and confirmed by PCR and Western blotting. Mutations in Dim1, Fap7, Tsr1, Pno1, and Rps14-expressing plasmids were introduced by site-directed mutagenesis, confirmed by sequencing.

Growth assays: Cell doubling times were measured in a Synergy 2 microplate reader (BioTek Instruments, Winooski, VT) as described (5). Statistical analyses were performed using Prism v.6.02 (GraphPad Software, La Jolla, CA).

Sucrose density gradient analysis: Sucrose gradient fractionations of whole cell lysates, followed by Northern blot analysis, were performed as described (4). 40S and 80S fractions 3-4 and 6-7 were quantified using Quantity One 1-D Analysis Software v.4.1.2 (Bio-Rad Laboratories, Hercules, CA). The 80S signal was divided by the sum of the 80S and 40S signals to calculate the 20S rRNA amount.

Antibodies: Antibodies against recombinant Dim1, Nob1, Pno1, Rio2, and Tsr1 were raised in rabbits (Josman, LLC, Napa, CA). Antibodies against Rpl3 or eEF2 were gifts from J. Warner. or T. Goss-Kinzy, respectively.

Protein expression/purification: MBP-Fap7(-RYD) was purified as described (5). Six-histidine tagged SUMO-Rps14(-RVM) was expressed in Rosetta DE3 cells, induced with 1 mM IPTG, and grown for 5 hours at 30˚C. Harvested cells were sonicated and cleared lysate was purified over Ni^{2+}-NTA resin per the manufacturer (Qiagen, Hilden, Germany), adding 0.5 mM PMSF and 1 mM benzamidine to buffers. Protein was dialyzed into 50 mM Tris pH 8.0/150 mM NaCl and purified using Mono S chromatography (GE LifeSciences, Chicago, IL), with gradient elution to 1.0 M NaCl. Final purification was on a Superdex 75 column in 50 mM Tris pH 8.0/200 mM NaCl/2 mM DTT/1 mM TCEP before protein was stored in buffer + 15% glycerol.

Protein binding: Protein binding assays were performed as described (5). 3 µM MBP-Fap7/MBP-Fap7-RYD was mixed with 4.4 µM SUMO-Rps14/SUMO-Rps14-RVM in binding buffer (BB, 50 mM Tris pH 7.5/150 mM NaCl/5% glycerol), applied to amylose resin, washed, and bound proteins eluted in BB + 50 mM maltose.

Cryo-EM: Fap7 was depleted by growth in YPD for 16 hours. 4 g frozen cell powder was suspended in 2.5 mL lysis buffer (30 mM HEPES-KOH pH 6.8/100 mM NaCl/6 mM $MgCl_2$ + RNasin and protease inhibitors) with 2 mL Zircona beads (Millipore-Sigma, St. Louis, MO) and vortexed. Lysate was cleared via centrifugation before incubation with 250 µL of IgG beads (GE Healthcare, Little Chalfonte, UK) at 4˚C for 1.5 h. Beads were washed with lysis buffer + 0.075% NP-40/PMSF/benzamidine followed by lysis buffer + PMSF/benzamidine then incubated with 250 µL lysis buffer + PMSF/benzamidine/1 mM DTT/0.5 mM EDTA/2.5 µL AcTEV protease (Invitrogen, Carlsbad, CA) at 16˚C for 2 h. After elution, the concentration was determined on a Nanodrop 1000 (ThermoFisher Scientific, Waltham, MA). 3 µL of 72 nM eluate was applied to a plasma-treated UltraAuFoil grid (Quantifoil, Großlöbichau, Germany). Grids were hand blotted before freezing in liquefied ethane.

Images were acquired on a ThermoFisher/FEI Titan Krios transmission electron microscope operating at 300 kV, equipped with a DE64 camera (Direct Electron, San Diego, CA) directed by the automated hole finder in Leginon (27). Images were recorded in "movie mode" at 1.3-2.5 µm defocus. 25 $e^-/Å^2$ dose was spread over 42 frames at a nominal magnification of 59,000x, yielding 1.24 Å/pixel at the specimen level. 4,193 micrographs were frame aligned and dose compensated with MotionCorr (28). Initial CTF parameters were estimated using Gctf (29). 146,641 particles were auto-picked in Relion-3.0, with per-particle CTF estimation/correction and beam-tilt correction (30). 3D classification revealed 55,949 80S particles (**Fig. S1**). 90,692 particles were 80S-like ribosomes (**Fig. S1, Table S2-5**).

Mature and 80S-like ribosomes were independently "autorefined" in Relion3.0 to 3.6 and 3.4 Å resolution, respectively (**Fig. S1**). The parent 80S-like structure revealed an anisotropic pre-40S (**Fig. S1**) so was further refined with a custom mask on either subunit, yielding structures of pre-40S and 60S at 3.7 and 3.4 Å-resolution, respectively (**Fig. S1**). The parent structure was subjected

to multi-body refinement in Relion-3.0 where 60S, including the bridge, was the first body and pre-40S was the second body with 11-Å overlapping masks (**Fig. S2**).

Local classification/refinement: Local classification was performed on a bin-2 stack using a spherical mask around H69. A dominant subclass (43,893 particles) was autorefined with masking on 60S to reveal the position of Dim1 (**Fig. S1b**). Although at lower resolution (~7.5 Å), the density has the size and shape of Dim1. H69 is resolved at ~5.5 Å and contours of its major and minor grooves are visible. Finally, the repositioned h24 has a resolution of ~8.5 Å and the twist of the helix is visible. These central elements are identifiable within the resolution limits because they connect to well-resolved parts of the structure; the distinct helical contours of the RNA; and the two-domain construction of Dim1.

Local classification was performed on a bin-2 stack using a spherical mask at the platform. A dominant class (36,914 particles) was autorefined with a mask on pre-40S (**Fig. S1b**). The platform density follows the contours of an unchanged Rps1•Rps14•Pno1 complex, supported by mutagenesis.

Modelling: 60S and pre-40S were modeled from the 80S ribosome (PDB 3J77, (31) using Chimera (32) to rigid body fit each subunit followed by manual adjustment in Coot (33). Rlp41, h23, h45, Rps1, Rps26, and Rps14 were removed with adjustments to Rpl19, H69, and the L1 stalk. In pre-40S, h24 was moved a rigid body to match the contours of the remodeled bridge. Additionally, the head RNA and proteins were positioned into that density. Tsr1 from PDB 6FAI (12) was fit as a rigid body. Yeast Dim1 was modeled in SwissModel (34) and, after rigid-body fitting into the bi-lobed density, α-helices and β-sheets were manually placed, followed by refinement with "Phenix.real.space.refine" (35). The model matched the density with a correlation coefficient (CC) of 0.8. Rps1•Rps14•Pno1 was fit into the segmented platform density, matching the density with a CC of 0.6. Each model was independently refined with "Phenix.real.space.refine" (35). Pre-40S had 89.7% residues in favored Ramachandran regions and 0.2% in outlier region (13% Clashscore). 60S had 85.9% residues in favored Ramachandran regions and 0.2% in outlier region (27.9% Clashscore).

Acknowledgments
This work was supported by NIH grants R01-GM117093 and R01-GM086451, and HHMI Faculty Scholar grant 55108536 to K.K.. The authors acknowledge the use of instruments at the Biological Science Imaging Resource supported by Florida State University and NIH grants S10 RR025080, S10 OD018142, and U24 GM116788. H.G. was supported in part by a PGA National Women's Cancer Awareness Postdoctoral Fellowship. We wish to thank members of the Karbstein lab for comments on the manuscript, and Drs. Scott Stagg and Kenneth Taylor for useful discussions. J.R. and H.G. prepared samples; J.R. and M.E.S. carried out structure reconstruction; M.D.P., H.H. and S.C. carried out yeast analyses; M.C.J. performed cryo-EM analysis of pre-40S; K.K. and M.E.S. conceived of the experiments and wrote the paper. Structure figures were made in Chimera and assembled in Photoshop (Adobe, San Jose, CA) without modification.

References:

1. J. Baßler, E. Hurt, Eukaryotic Ribosome Assembly. *Annu Rev Biochem* **88**, 281-306 (2019).
2. S. Klinge, J. L. Woolford, Ribosome assembly coming into focus. *Nat Rev Mol Cell Biol* **20**, 116-131 (2019).

3. S. Lebaron *et al.*, Proofreading of pre-40S ribosome maturation by a translation initiation factor and 60S subunits. *Nat Struct Mol Biol* **19**, 744-753 (2012).
4. B. S. Strunk, M. N. Novak, C. L. Young, K. Karbstein, A translation-like cycle is a quality control checkpoint for maturing 40S ribosome subunits. *Cell* **150**, 111-121 (2012).
5. H. Ghalei *et al.*, The ATPase Fap7 Tests the Ability to Carry Out Translocation-like Conformational Changes and Releases Dim1 during 40S Ribosome Maturation. *Mol Cell* **68**, 1155 (2017).
6. J. Barandun *et al.*, The complete structure of the small-subunit processome. *Nat Struct Mol Biol* **24**, 944-953 (2017).
7. J. Cheng, N. Kellner, O. Berninghausen, E. Hurt, R. Beckmann, 3.2-Å-resolution structure of the 90S preribosome before A1 pre-rRNA cleavage. *Nat Struct Mol Biol* **24**, 954-964 (2017).
8. Q. Sun *et al.*, Molecular architecture of the 90S small subunit pre-ribosome. *Elife* **6** (2017).
9. M. Ameismeier, J. Cheng, O. Berninghausen, R. Beckmann, Visualizing late states of human 40S ribosomal subunit maturation. *Nature* **558**, 249-253 (2018).
10. A. Heuer *et al.*, Cryo-EM structure of a late pre-40S ribosomal subunit from. *Elife* **6** (2017).
11. M. C. Johnson, H. Ghalei, K. A. Doxtader, K. Karbstein, M. E. Stroupe, Structural Heterogeneity in Pre-40S Ribosomes. *Structure* **25**, 329-340 (2017).
12. A. Scaiola *et al.*, Structure of a eukaryotic cytoplasmic pre-40S ribosomal subunit. *EMBO J* **37** (2018).
13. B. S. Strunk *et al.*, Ribosome assembly factors prevent premature translation initiation by 40S assembly intermediates. *Science* **333**, 1449-1453 (2011).
14. H. Ghalei *et al.*, Hrr25/CK1delta-directed release of Ltv1 from pre-40S ribosomes is necessary for ribosome assembly and cell growth. *J Cell Biol* **208**, 745-759 (2015).
15. T. Nakane, D. Kimanius, E. Lindahl, S. H. Scheres, Characterisation of molecular motions in cryo-EM single-particle data by multi-body refinement in RELION. *Elife* **7** (2018).
16. R. D. Pai *et al.*, Structural Insights into ribosome recycling factor interactions with the 70S ribosome. *J Mol Biol* **376**, 1334-1347 (2008).
17. M. A. Borovinskaya *et al.*, Structural basis for aminoglycoside inhibition of bacterial ribosome recycling. *Nat Struct Mol Biol* **14**, 727-732 (2007).
18. I. Prokhorova *et al.*, Aminoglycoside interactions and impacts on the eukaryotic ribosome. *Proc Natl Acad Sci U S A* **114**, E10899-E10908 (2017).
19. L. Wang *et al.*, Allosteric control of the ribosome by small-molecule antibiotics. *Nat Struct Mol Biol* **19**, 957-963 (2012).
20. A. Ben-Shem *et al.*, The structure of the eukaryotic ribosome at 3.0 Å resolution. *Science* **334**, 1524-1529 (2011).
21. U. M. McCaughan *et al.*, Pre-40S ribosome biogenesis factor Tsr1 is an inactive structural mimic of translational GTPases. *Nat Commun* **7**, 11789 (2016).
22. I. S. Fernández *et al.*, Molecular architecture of a eukaryotic translational initiation complex. *Science* **342**, 1240585 (2013).

23. Z. Lu *et al.*, Gas-Assisted Annular Microsprayer for Sample Preparation for Time-Resolved Cryo-Electron Microscopy. *J Micromech Microeng* **24**, 115001 (2014).
24. J. Loc'h *et al.*, RNA mimicry by the fap7 adenylate kinase in ribosome biogenesis. *PLoS Biol* **12**, e1001860 (2014).
25. U. A. Hellmich *et al.*, ssential ribosome assembly factor Fap7 regulates a hierarchy of RNA-protein interactions during small ribosomal subunit biogenesis. *Proc Natl Acad Sci U S A* **110**, 15253-15258 (2013).
26. M. S. Longtine *et al.*, Additional modules for versatile and economical PCR-based gene deletion and modification in Saccharomyces cerevisiae. *Yeast* **14**, 953-961 (1998).
27. B. Carragher *et al.*, Leginon: an automated system for acquisition of images from vitreous ice specimens. *J Struct Biol* **132**, 33-45 (2000).
28. X. Li *et al.*, Electron counting and beam-induced motion correction enable near-atomic-resolution single-particle cryo-EM. *Nat Methods* **10**, 584-590 (2013).
29. K. Zhang, Gctf: Real-time CTF determination and correction. *J Struct Biol* **193**, 1-12 (2016).
30. J. Zivanov *et al.*, New tools for automated high-resolution cryo-EM structure determination in RELION-3. *Elife* **7** (2018).
31. E. Svidritskiy, A. F. Brilot, C. S. Koh, N. Grigorieff, A. A. Korostelev, Structures of yeast 80S ribosome-tRNA complexes in the rotated and nonrotated conformations. *Structure* **22**, 1210-1218 (2014).
32. E. F. Pettersen *et al.*, UCSF Chimera - A visualization system for exploratory research and analysis. *Journal of Computational Chemistry* **25**, 1605-1612 (2004).
33. P. Emsley, B. Lohkamp, W. G. Scott, K. Cowtan, Features and development of Coot. *Acta Crystallogr D Biol Crystallogr* **66**, 486-501 (2010).
34. A. Waterhouse *et al.*, SWISS-MODEL: homology modelling of protein structures and complexes. *Nucleic Acids Res* **46**, W296-W303 (2018).
35. P. D. Adams *et al.*, PHENIX: a comprehensive Python-based system for macromolecular structure solution. *Acta Crystallogr D Biol Crystallogr* **66**, 213-221 (2010).

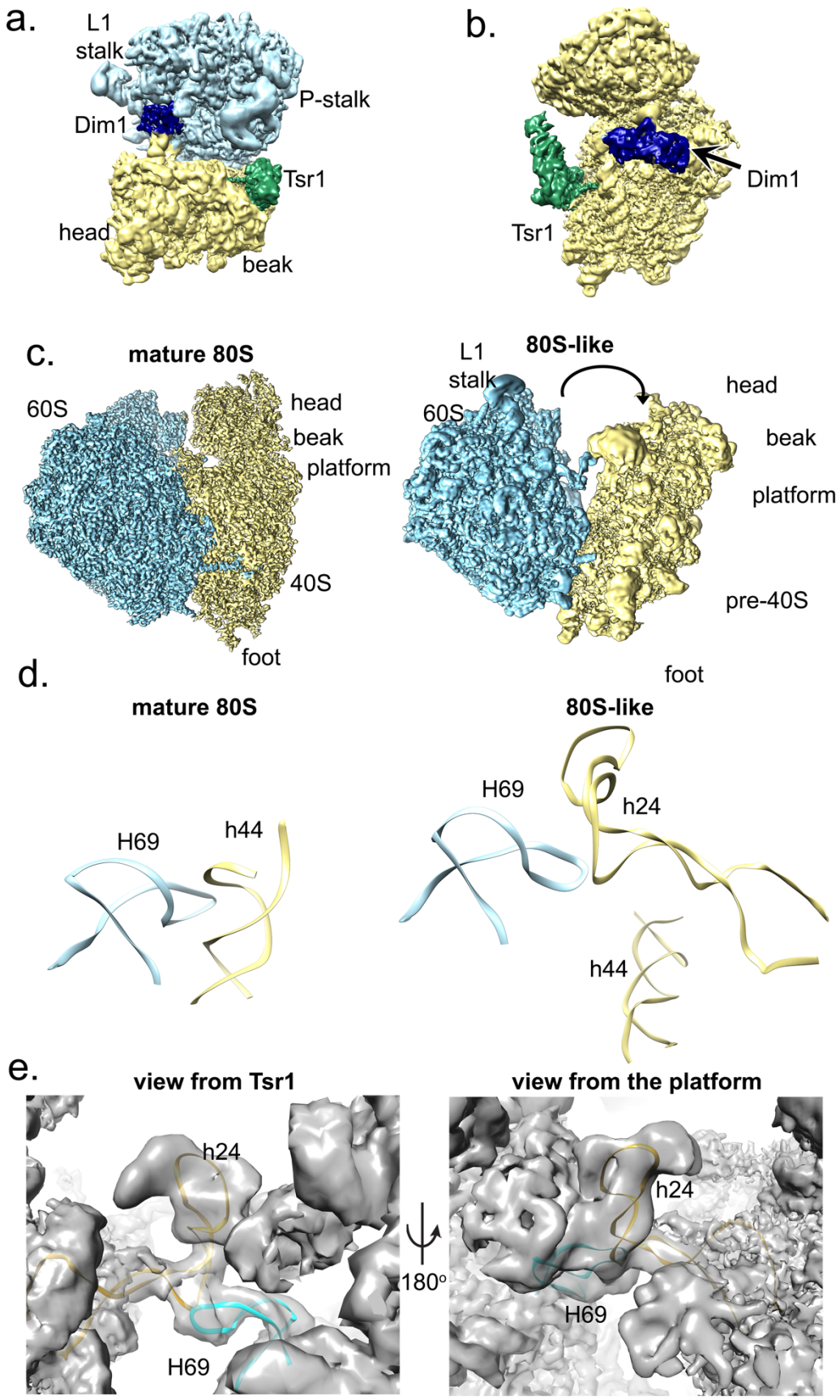
a.
L1
stalk
P-stalk
Dim1
Tsr1
head
beak
b.
Dim1
Tsr1
c.
mature 80S
60S
head
beak
platform
40S
foot
80S-like
L1
stalk
60S
head
beak
platform
pre-40S
foot
d.
mature 80S
H69
h44
80S-like
H69
h24
h44
e.
view from Tsr1
h24
H69
180°
view from the platform
h24
H69

Fig. 1: 80S-like ribosomes join via an immature interface. a. Overall structure of 80S-like ribosomes. 60S is light blue, pre-40S is yellow, Dim1 is dark blue, and Tsr1 is green. **b.** The pre-40S interface has only Tsr1 (green) and Dim1 (blue) bound. **c.** In 80S-like pre-ribosomes the space between the subunits is expanded. **d.** In mature ribosomes, helix 69 from the 60S subunit (H69, blue) binds helix 44 from the pre-40S subunit (h44, yellow, model from PDB ID 3J77 (31)). 80S-like ribosomes join through a novel bridge B2a/c where H69 (blue) joins a repositioned h24 (yellow). **e.** H69 and h24 fit into the density at the subunit interface.

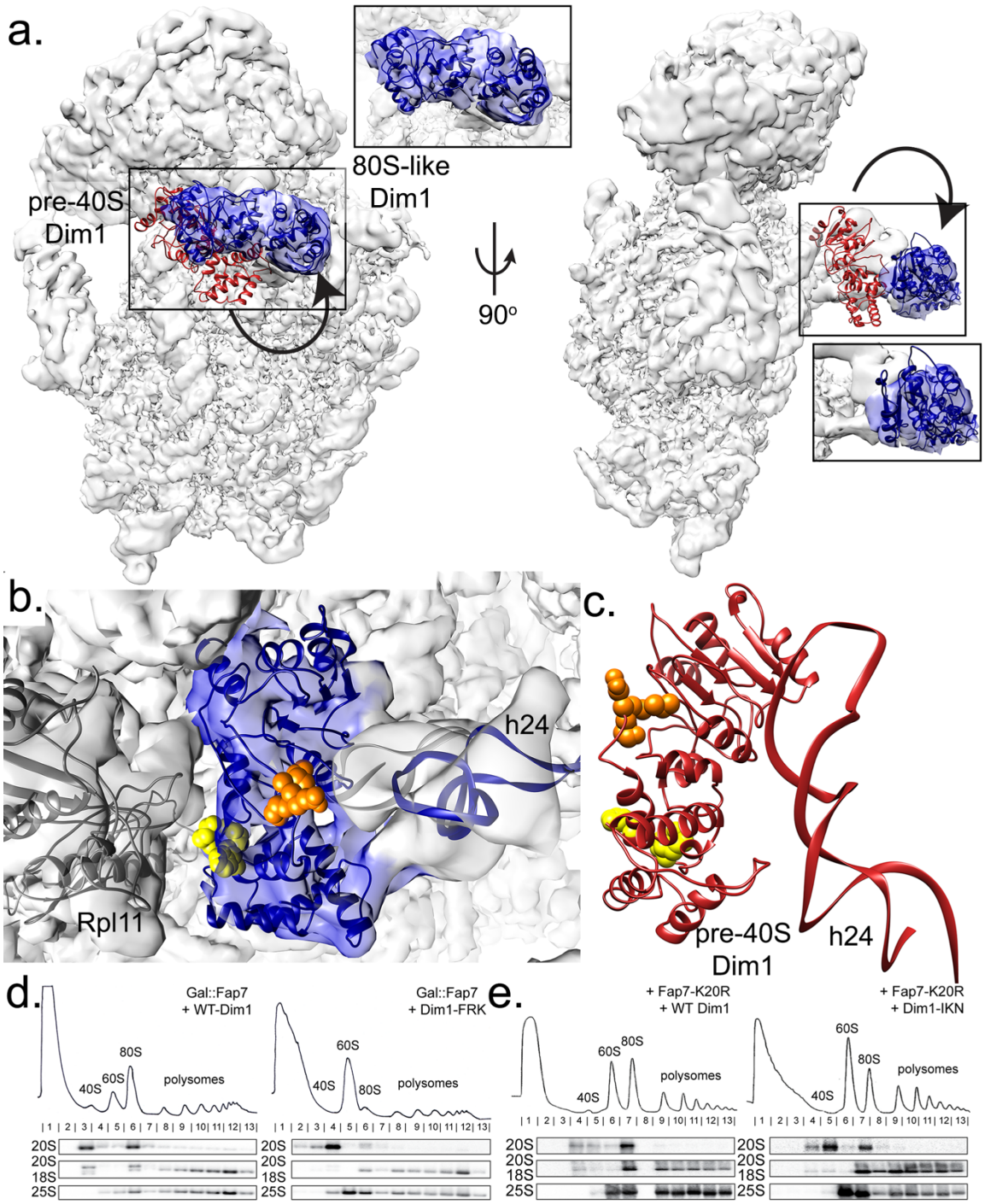

Fig. 2: Dim1 stabilizes h24 at the 80S-like pre-ribosome interface. a. Local classification followed by refinement and local B-factor sharpening in Relion-3.0 revealed a bi-lobed density at the 60S-pre-40S interface that matches the Dim1 structure (blue). The position of Dim1 in an earlier cytoplasmic pre-40S intermediate (red, Dim1 fit into EMD-4218 (13)) is also shown, demonstrating its repositioning at the interface. **b.** Phe231, Arg233, and Lys234 (Dim1-FRK) (orange) face h24. Ile250, Lys253 and Asn254 (Dim1-IKN) (yellow) face Rpl11 in the 60S subunit. **c.** Phe231,

Arg233, and Lys234 (orange) and Ile250, Lys253 and Asn254 (yellow) do not face any structural elements in pre-40S subunits. **d.** Dim1-FRK blocks subunit joining. Whole cell extracts from cells depleted of endogenous Dim1 and Fap7 (Gal::Dim1;Gal::Fap7) for 16-20 h and supplemented with plasmids encoding wild type or mutant Dim1 were fractionated on 10-50% sucrose gradients and the sedimentation of pre-40S ribosomes containing 20S rRNA were probed by Northern blot analysis. 80S-like ribosomes sediment in fractions 6-7 and contain 20S and 25S rRNA. Blocking the formation of 80S-like ribosomes will lead to sedimentation of pre-40S (without 25S rRNA) in fractions 3-5 (4, 5, 14). **e.** Dim1-IKN impairs subunit joining. Dim1 and Fap7 were depleted for 16-20 h and cells were supplemented with plasmids encoding Fap7-K20R (inactive Fap7) and wild type or mutant Dim1 as indicated.

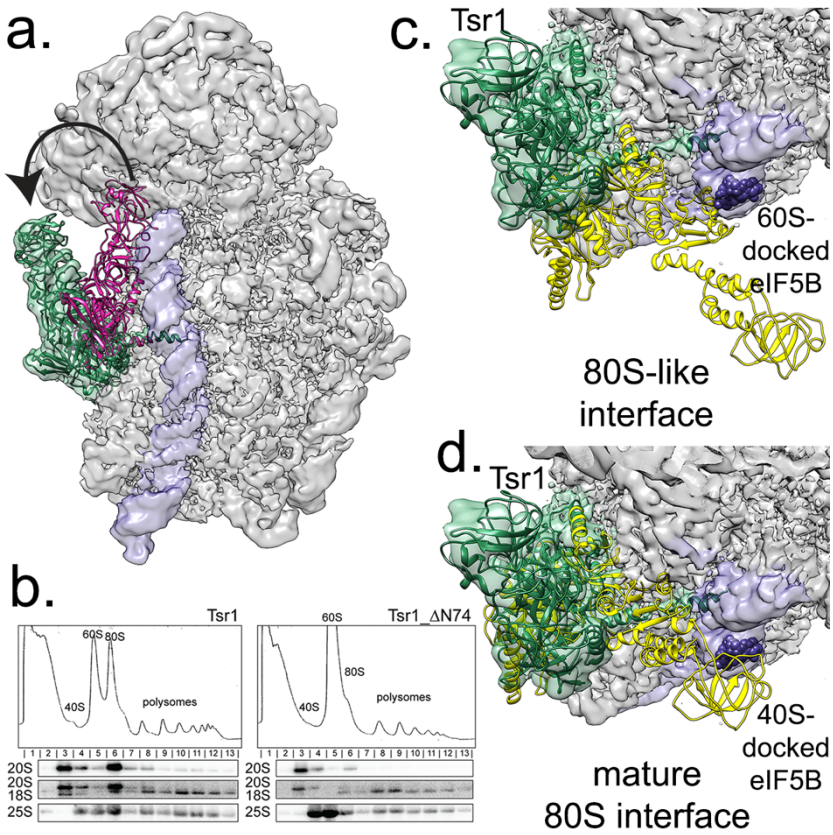

Figure 3: Tsr1 is repositioned to the beak. a. The position of Tsr1 in 80S-like ribosomes (green) is substantially different from the position previously identified in an earlier cytoplasmic pre-40S intermediate (pink), rotated away from the head but still interacting with h44 (purple) (Model from EMD-8349 (11)). **b.** Whole cell extracts from cells in panel c were fractionated on 10-50% sucrose gradients and fractions were probed by Northern blot. **c.** The opened pre-40S and 60S interface leaves space for eIF5B (yellow) across h44 (purple), blocking the early-forming B3 bridge (marked by nucleotides 1655-1657, shown as purple spheres). Model was obtained by superimposition of the 60S subunits from the 80S-like pre-ribosome structure here and the eIF5B-bound mature 80S ribosome (PDB ID 4V8Z (22)). **d.** If subunits were joining in the canonical mature 80S-structure, Tsr1 binding would block eIF5B recruitment. Model was obtained by superimposition of the 40S subunits from the 80S-like pre-ribosome structure here and the eIF5B-bound mature 80S ribosome (PDB ID 4V8Z (22)). The clashscore, as defined in Phenix (35) as the number of overlaps greater than 0.4 Å/1000 atoms, increases from 170 when 60S is superimposed to position eIF5B to 780 when 40S is superimposed to position eIF5B, an increase from 2% to 11% of the total atoms in Tsr1.

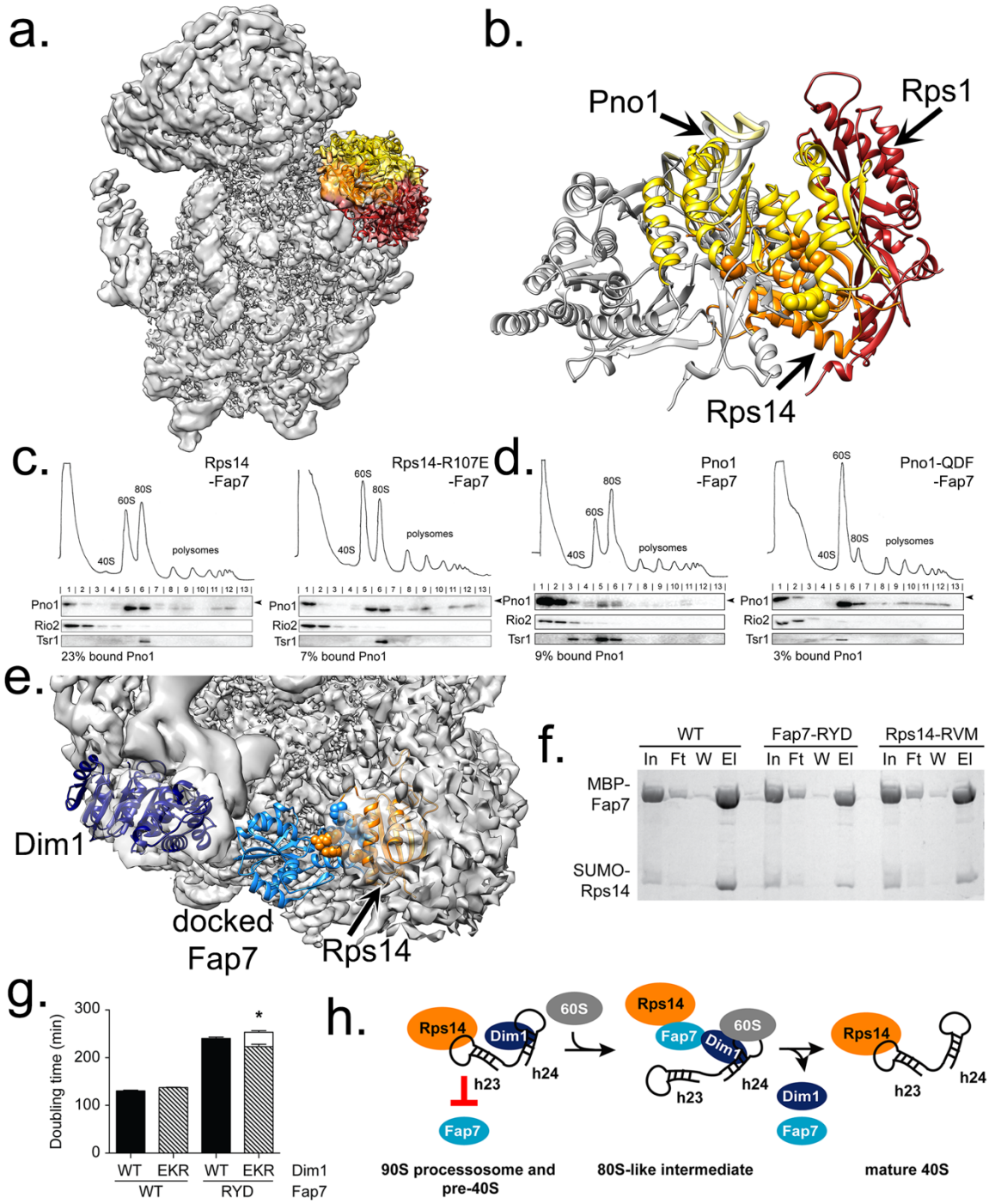

Figure 4: The pre-40S platform is opened to enable Fap7 recruitment to 80S-like ribosomes. **a.** After local classification at the platform, alignment, and local B-factor sharpening in Relion-3.0, the dominant class has density that corresponds to Rps1 (red), Rps14 (orange), and Pno1 (yellow) albeit not at their final position. **b.** In 80S-like ribosomes Rps1 (red), Rps14 (orange) and Pno1 (yellow) are shifted outwards relative to their positions in an earlier pre-40S intermediate (PDB ID 6FAI (12), Rps1, Rps14, and Pno1 in gray). **c.** Whole cell extracts from cells depleted of Fap7 and containing wild type Rps14 or Rps14-R107E were fractionated on 10-50% sucrose gradients and

fractions were probed by Western blot. Bound Pno1 was calculated as the percent of Pno1 in fractions 4-13 compared to total Pno1. **d.** Whole cell extracts from cells depleted of Fap7 and containing wild type Pno1 or Pno1-QDF were fractionated on 10-50% sucrose gradients and fractions were probed by Western blot. Bound Pno1 was calculated as in **c**. **e.** Docking Fap7•Rps14 (Fap7, chain G and Rps14, chain F) from PDB ID 4CW7 (24) onto Rps14 (orange) in 80S-like ribosomes places Fap7 (cyan) in direct contact with Dim1 (blue), as predicted by previous biochemical data (5). Residues R114, Y116, D118 in Fap7 (Fap7-RYD, shown in orange), R41, V42, M46 (Rps14-RVM,/K49E shown in blue) in Rps14 are at the interface between Fap7 and Rps14, that is formed between chains G and F). **f.** Interface mutations in Fap7 or Rps14 weaken their binding affinity for each other. Shown are Coomassie-stained SDS-PAGE gels of protein binding assays on amylose beads of purified, recombinant MBP-Fap7 or MBP-Fap7-RYD and SUMO-Rps14 or SUMO-Rps14-RVM. In, input; Ft, flow-through; W, final wash; El, elution. **g.** Doubling time, in minutes, of cells depleted of endogenous Dim1 and Fap7 (Gal::Dim1; Gal::Fap7) and transformed with plasmids encoding wild type or Dim1-EKR (E93R; K96D; R97E) and either wild type Fap7 or Fap7-RYD. The white column represents the expected doubling time if there was no rescue of Fap7-RYD by Dim1-EKR (See also (5)). The height of this column was calculated by multiplying the observed fold differences for each single mutation (RYD with EKR). The data are the average of 16-17 biological replicates and the error bars represent SEM. Unpaired t-test was performed comparing expected and actual doubling times of cells expressing Fap7-RYD and Dim1-EKR. *p-value = 0.030. **h**. The Fap7 binding site on Rps14 is blocked by h23 in nucleolar 90S processosomes (6-8), and earlier 40S assembly intermediates (10, 12). Opening of the platform temporarily removes h23, enabling Fap7 recruitment to promote Dim1 release (5).